

## Microstructural length scale parameters to model the high-cycle fatigue behaviour of notched plain concrete

*O. Jadallah, C. Bagni, H. Askes and L. Susmel*

Department of Civil and Structural Engineering, The University of Sheffield,  
Sheffield S1 3JD, United Kingdom

**Corresponding Author:** Prof. **Luca Susmel**  
Department of Civil and Structural Engineering  
The University of Sheffield, Mappin Street, Sheffield, S1 3JD, UK  
Telephone: +44 (0) 114 222 5073  
Fax: +44 (0) 114 222 5700  
e-mail: [l.susmel@sheffield.ac.uk](mailto:l.susmel@sheffield.ac.uk)

### Abstract

The present paper investigates the importance and relevance of using microstructural length scale parameters in estimating the high-cycle fatigue strength of notched plain concrete. In particular, the accuracy and reliability of the Theory of Critical Distances and Gradient Elasticity are checked against a number of experimental results generated by testing, under cyclic bending, square section beams of plain concrete containing stress concentrators of different sharpness. The common feature of these two modelling approaches is that the required effective stress is calculated by using a length scale which depends on the microstructural material morphology. The performed validation exercise demonstrates that microstructural length scale parameters are successful in modelling the behaviour of notched plain concrete in the high-cycle fatigue regime.

**Keywords:** microstructural length scale, fatigue, notch, plain concrete

### NOMENCLATURE

a	Crack-length (or semi-crack length)
d	Specimen depth
$f_T, f_C, f_B$	Static strength determined under tension, compression and bending
k	S-N curve's negative inverse slope
$l$	Intrinsic material length scale determined according to GM
$r_n$	Notch root radius
t	Time
w	Specimen width
$K_t$	Net stress concentration factor
K, $\delta$	Constants in Dixon's equation
L	Intrinsic material length scale determined according to TCD
M(t)	Cyclic bending moment
$N_f$	Number of cycles to failure
$N_0$	Reference number of cycles to failure
Oxyz	System of coordinates
P(t)	Cyclic axial force
$P_S$	Probability of survival
R	Load ratio ( $R = \sigma_{\min} / \sigma_{\max}$ )

$T_{\sigma}$	Scatter ratio of the endurance limit for 90% and 10% probabilities of survival.
$\theta, r$	Polar coordinates
$\sigma_{o,MAX}$	Maximum value of the un-notched endurance limit
$\sigma_1$	Local maximum principal stress
$\sigma_{1,max}$	Maximum value of local stress component $\sigma_1$
$\sigma_a$	Stress amplitude
$\sigma_{Design}$	Design stress
$\sigma_{eff,max}$	Maximum value of the effective stress
$\sigma_{GEo,max}$	Maximum value of the endurance limit determined via GE
$\sigma_{LT}$	Stress level characterising the last test run according to Dixon's method
$\sigma_m$	Mean stress
$\sigma_{max}$	Maximum stress
$\sigma_{MAX}$	Maximum value of the endurance limit for $\sigma_{max} > 0$
$ \sigma_{MIN} $	Absolute minimum value of the endurance limit for $\sigma_{max} \leq 0$
$\sigma_{min}$	Minimum stress
$\sigma_S$	Reference static strength
$\sigma_y$	Local stress parallel to axis y
$\sigma_{y,max}$	Maximum value of stress component $\sigma_y$
$\Delta K_{th}$	Threshold value of the stress intensity factor range
$\Delta \sigma_1$	Range of the maximum principal stress
$\Delta \sigma_{eff}$	Range of the effective stress
$\Delta \sigma_y$	Range of stress component $\sigma_y$
$\Delta \sigma_o$	Range of the un-notched endurance limit

## 1. Introduction

As reported by the World Business Council for Sustainable Development (<http://www.wbcsd.org>), concrete is the most widely used structural material. Consequently, the continuous development of the civil infrastructure sector requires the production of about 2.35 billion tons of concrete per year. From a green-design point of view, one of the most urgent issues to be addressed is the improvement of the in-service performance of concrete structures by simultaneously reducing the production, maintenance and energy costs, as well as a reduction of carbon emissions. In this setting, performing the static assessment of concrete structures has been investigated for decades by the international scientific community, and concrete structures nowadays can efficiently be designed against static loading by adopting relatively low safety factors. This results in slender structures, allowing a markedly reduced usage of natural resources with positive effects on sustainability and carbon emissions.

However, a decrease in the size of concrete structural components leads to an inevitable increase of the magnitude of in-service local stresses, making concrete structures more susceptible to fatigue. As far as both plain and short-fibre/particle reinforced concretes are concerned, in a recent investigation [1] it has been proven that, when the design is performed by using safety factors lower than 2.5, the presence of time-variable loading can no longer be ignored. This aspect is important because several key concrete structures undergo in-service time-variable loading, such as, for instance, runways subjected to repeated loads due to passing aircrafts, asphalt concretes subjected to cyclic local pressures due to the action of tyres, bridges fatigued by travelling vehicles, and concrete foundations of wind turbines. Further, in 2012 a British working group [2] operating under the auspices of both the Department of Energy and Climate Change and the Office for Nuclear Development has explicitly indicated fatigue as one of the key structural issues to be addressed when designing concrete structures for the nuclear sector. In this scenario, properly performing the fatigue assessment of concrete infrastructures is complicated by the fact that their structural parts experience stress/strain concentration phenomena due to local geometrical features (here termed “notches”).

To rationalise the usage of natural resources and minimise carbon emissions, structural engineers will increasingly be requested to design structural components by using the least amount of material needed to reach an adequate level of safety. This would result in the design of concrete structural parts/details having complex shape, with such geometrical features inevitably causing localised stress/strain concentration phenomena. These considerations clearly indicate that fatigue of notched concrete is a research area which is expected to become more and more important in the near future. However, examination of the state-of-the-art suggests that, apart from three isolated investigations [3-5], the problem of assessing notched concretes against fatigue has not been studied systematically before.

As far as un-cracked/un-notched concrete structures are concerned, since the early 1900s [6, 7] the international scientific community has investigated the fatigue behaviour of plain

concrete mainly from an experimental point of view (see Ref. [1] for an up-to-date summary of the data available in the technical literature). Unfortunately, in spite of such a large body of experimental work, no universally accepted design technique yet exists. Perhaps, slightly crudely, it can be said that the experimental work carried out so far has resulted in S-N curves which can be used to design against fatigue solely for those specific concretes that were tested.

In plain concrete cracks can typically initiate in the cement paste, inside the aggregates, or at the interface between matrix and aggregates [8, 9]. The last cracking mechanism is seen to be the prevailing one in case of fatigue; consequently, fatigue cracks originate as a result of a progressive deterioration of the bonds under local tensile/shear cyclic stresses and strains [10]. According to this fatigue damage model, aggregates play the role of hard inclusions causing localised stress/strain concentration phenomena. These considerations suggest that the material microstructural features play a primary role in defining the overall fatigue strength of plain concrete. When using continuum mechanics theories to predict the fatigue behaviour of concrete structures or components, it is therefore important that such microstructural features are taken into account properly. In this complex scenario, the aim of the present paper is to investigate the applicability and accuracy of two continuum mechanics theories that make use of a microstructural length scale parameter – i.e., the Theory of Critical Distances (TCD) and Gradient Elasticity (GE) – in modelling the high-cycle fatigue behaviour of notched plain concrete.

## **2. Preliminary definitions and assumptions**

The fatigue strength of plain concrete is seen to depend on several variables which include surface roughness, extreme environmental conditions, temperature, type of loading, load history's degree of multiaxiality, water-to-cement ratio, ageing, and presence of shrinkage stresses.

Given the material and the environmental conditions, from a design point of view, the overall fatigue strength of a concrete structure is strongly affected also by the presence of non-zero mean stresses [1]. This implies that the stress quantities to be used to apply both the TCD and GE must be defined so that the mean stress effect in concrete fatigue is taken into account effectively.

To determine the stress quantities of interest, it is important to point out from the start that, in the present study, tensile stresses are taken as positive and compressive stresses as negative.

Consider the beam sketched in Figure 1 which is hypothesised to be damaged either by a cyclic bending moment  $M(t)$  (Fig. 1a) or by a cyclic axial force  $P(t)$  (Fig. 1b),  $t$  being time. Point O is the location where a fatigue crack is expected to initiate, so that this material point is used also to define a convenient system of coordinates (see Figures 1a and 1b). Time-variable force  $P(t)$  and bending moment  $M(t)$  result in a local stress at point O that varies cyclically as shown in the  $\sigma_y$  vs.  $t$  charts reported in Figures 1c and 1d, respectively. As soon as the amplitude,  $\sigma_a$ , the mean value,  $\sigma_m$ , the maximum stress,  $\sigma_{max}$ , and the minimum stress,  $\sigma_{min}$ , characterising the loading cycle are known (see Figures 1c and 1d), the corresponding load ratio,  $R$ , can directly be defined as follows [11]:

$$R = \frac{\sigma_m - \sigma_a}{\sigma_m + \sigma_a} = \frac{\sigma_{min}}{\sigma_{max}} \quad (1)$$

Definition (1) suggests that, as long as the maximum stress is positive (Fig. 1c), the load ratio takes on a value which is always lower than unity, a negative minimum stress resulting in a negative value for  $R$ . On the contrary, when the concrete component being assessed is subjected to cyclic compression (Fig. 1d),  $R$  takes on a value which is always larger than unity,  $R$  diverging to infinity as  $\sigma_{max}$  approaches zero.

By reanalysing about 1500 experimental results taken from the literature and generated by testing both plain and short-fibre/particle reinforced concretes [1], it has been proven that the mean stress effect in concrete fatigue can efficiently be modelled by defining the design stress,  $\sigma_{\text{Design}}$ , as follows:

$$\sigma_{\text{Design}} = \sigma_{\text{max}} \quad \text{when } \sigma_{\text{max}} > 0 \quad (2)$$

$$\sigma_{\text{Design}} = |\sigma_{\text{min}}| \quad \text{when } \sigma_{\text{max}} \leq 0 \quad (3)$$

The fatigue strength of concrete can then be summarised in conventional log-log S-N diagrams, where the design stress,  $\sigma_{\text{Design}}$ , is plotted against the number of cycles to failure,  $N_f$  (Fig. 1e). According to this schematisation, fatigue results can directly be post-processed through appropriate statistical tools [11, 12] to determine the corresponding fatigue curve for the targeted probability of survival,  $P_s$ . Irrespective of the adopted value for  $P_s$ , fatigue curves can be described mathematically as follows:

$$\sigma_{\text{Design}}^k \cdot N_f = \sigma_0^k \cdot N_0 \quad (4)$$

where  $k$  is the negative inverse slope and  $\sigma_0$  is the design endurance limit, i.e., a reference strength extrapolated at a reference number of cycles to failure,  $N_0$  (see Figure 1e).

The level of scattering associated with the investigated data set can concisely be quantified by using the following ratio [11]:

$$T_\sigma = \frac{\sigma_{0,10\%}}{\sigma_{0,90\%}} \quad (5)$$

where  $\sigma_{0,10\%}$  and  $\sigma_{0,90\%}$  are the endurance limits determined, at  $N_0$  cycles to failure, for 10% and 90% probabilities of survival, respectively. According to definitions (2) and (3), design endurance limits,  $\sigma_0$ , are then suggested to be defined as [1]:

$$\sigma_0 = \sigma_{\text{MAX}} \quad \text{when } \sigma_{\text{max}} > 0 \quad (6)$$

$$\sigma_0 = |\sigma_{\text{MIN}}| \quad \text{when } \sigma_{\text{max}} \leq 0 \quad (7)$$

In the above definitions  $\sigma_{\text{MAX}}$  and  $|\sigma_{\text{MIN}}|$  are determined at  $N_0$  cycles to failure.

As demonstrated in the fatigue diagram reported in Figure 1f, the assumptions discussed above allow a unifying scatter band suitable for designing un-notched concretes against fatigue to be determined. In more detail, this scatter band was determined by post-processing about 1500 experimental data taken from the literature and generated by testing both plain and short-fibre/particle reinforced concretes cyclically loaded either in tension, in tension-compression, in compression, or in bending [1]. Such a high level of unification was reached by normalising the design stress,  $\sigma_{\text{Design}}$ , via the pertinent reference static strength,  $\sigma_s$ , defined as follows:

- under cyclic tension-tension/compression  $\Rightarrow \sigma_s = f_T$
- under cyclic compression  $\Rightarrow \sigma_s = f_C$
- under cyclic bending  $\Rightarrow \sigma_s = f_B$

In the above definitions  $f_T$ ,  $f_C$ , and  $f_B$  are the material static strengths determined under tension, compression, and bending, respectively. The fatigue curve reported in Figure 1 was determined under the hypothesis of a log-normal distribution of the number of cycles to failure for each stress level by assuming a confidence level equal to 95% [12]

It is worth observing here that, according to the available design codes [13, 14], the reference fatigue curves recommended to perform the fatigue assessment of welded joints are characterised by a  $T_0$  value equal to 1.5 [15]. As shown in Figure 1f, the  $T_0$  value associated with the reported unifying scatter band is equal to 1.418, which confirms the validity of the formed hypotheses. Therefore, according to Figure 1f, the fatigue lifetime of un-notched plain and short-fibre/particle reinforced concrete can directly be estimated by using solely the pertinent material static strength,  $\sigma_s$ , as calibration information independently from the actual value of the mean stress characterising the load history being assessed.

Since the schematisation summarised in the present section has proven to be capable of accurately taking into account the mean stress effect in concrete fatigue, the same strategy - i.e., definitions (6) and (7) - will be used in what follows not only to reformulate both the TCD and GE to make them suitable for modelling the high-cycle fatigue behaviour of notched plain concretes, but also to post-process the generated experimental results.

### **3. Fundamentals of the Theory of Critical Distances**

The TCD postulates that the high-cycle fatigue strength of notched/cracked materials can directly be estimated through the local linear-elastic stress fields damaging the material in the vicinity of the assessed geometrical features [16-18]. Examination of the state of the art [19] suggests that, since about the middle of the last century, this idea has been formalised in different ways by simply changing the shape and size of the reference integration domain [20]. The common feature of these different formalisations of the TCD is that the effective stress used to estimate the fatigue damage extent depends on a microstructural length scale parameter,  $L$ , which takes on the following value [18, 21]:

$$L = \frac{1}{\pi} \left( \frac{\Delta K_{th}}{\Delta \sigma_0} \right)^2 \quad (8)$$

where  $\Delta K_{th}$  is the range of the threshold value of the stress intensity factor and  $\Delta\sigma_o$  is the range of the un-notched endurance limit (both determined under the same load ratio,  $R$ , as the one damaging the component being assessed). According to definition (8), the TCD makes use of fatigue property  $\Delta K_{th}$  to estimate the required critical distance. It is worth remembering here that the Linear-Elastic Fracture Mechanics concepts can successfully be used to model the cracking behaviour of plain concrete provided that the size of the assessed component is large enough to allow the mix to be treated as a homogenous material [22].

In order to formalise the TCD mathematically, consider the notched component sketched in Figure 2a which is assumed to be subjected to cyclic axial force  $P(t)$ . The Volume Method (VM) [18, 20], which represents the most complex way of using the TCD, assumes that the range of the effective stress,  $\Delta\sigma_{eff}$ , has to be calculated by averaging the range of the maximum principal stress,  $\Delta\sigma_1$ , over an hemisphere centred at the notch tip. The complexity of the problem can be reduced by simply using a bi-dimensional integration domain. In particular, according to the Area Method (AM) [18],  $\Delta\sigma_{eff}$  can be calculated by averaging  $\Delta\sigma_1$  over a semi-circular area centred at the apex of the geometrical feature being assessed, i.e. (see also Figure 2b):

$$\Delta\sigma_{eff} = \frac{4}{\pi L^2} \int_0^{\pi/2} \int_0^L \Delta\sigma_1(\theta, r) \cdot r \cdot dr \cdot d\theta \quad (9)$$

where  $L$  is the material critical distance estimated via definition (8).

By using the VM/AM argument, the assumption can be made that the high-cycle fatigue strength of notched/cracked materials is related to the linear-elastic stress field acting on the so-called structural volume [16], such a process zone becoming the portion of material controlling the overall high-cycle fatigue strength of the component being designed. Therefore, according to the VM and AM's *modus operandi*, the radius of the volume/area delimiting the process zone itself can be assumed to approach critical distance  $L$ . As far as

high-cycle fatigue damage is concerned, the size of the structural volume is seen to depend on the material microstructural features as well as on the characteristics of the physical processes leading to the initiation of fatigue cracks [23]. Thus, length scale parameter  $L$  is related to the local morphology of the material being assessed.

From a practical point of view, the in-field usage of both the VM and AM is complicated by the fact that specific numerical/analytical techniques are required to average  $\Delta\sigma_1$  over the appropriate integration domain. However, following a fairly articulated reasoning based on the Linear-Elastic Fracture Mechanics concepts [18], the problem can be simplified by proving that  $\Delta\sigma_{\text{eff}}$  is also equal to the stress range at a distance from the notch/crack tip equal to  $L/2$  (Fig. 2c). In other words, the stress state calculated at the centre of the process zone is seen to be capable of giving an information suitable for accurately quantifying the damage extent associated with the entire process zone. This simplified formalisation of the TCD is known as the Point Method (PM) [17, 18], the corresponding effective stress range taking on the following value (see also Figure 2c):

$$\Delta\sigma_{\text{eff}} = \Delta\sigma_y \left( \theta = 0^\circ, r = \frac{L}{2} \right) \quad (10)$$

Another simplified way of using the TCD is known as the Line Method (LM) [16, 18]. The LM postulates that  $\Delta\sigma_{\text{eff}}$  has to be calculated by averaging  $\Delta\sigma_y$  over a straight line having length equal to  $2L$ , i.e. (Fig. 2d):

$$\Delta\sigma_{\text{eff}} = \frac{1}{2L} \int_0^{2L} \Delta\sigma_y(\theta = 0^\circ, r) dr \quad (11)$$

Irrespective of the strategy followed to calculate  $\Delta\sigma_{\text{eff}}$ , the notched component being assessed is supposed to be in the endurance limit condition as long as the range of the effective stress is lower than (or, at least, equal to) the un-notched material endurance limit (i.e.,  $\Delta\sigma_{\text{eff}} \leq \Delta\sigma_o$ ).

The most important features of the TCD were summarised above by forming the assumption that the value of the microstructural length scale parameter,  $L$ , is known *a priori*. According to definition (8),  $L$  can directly be derived provided that the range of the threshold value of the stress intensity factor,  $\Delta K_{\text{th}}$ , is determined by running appropriate experiments. If this is not possible,  $L$  can also be estimated through an endurance limit experimentally obtained by testing specimens containing a known geometrical feature [24], the use of notches as sharp as possible being always advisable [11]. According to Figure 2e, the stress-distance curve plotted along the bisector of the investigated notch and the un-notched endurance limit allow  $L$  to be estimated directly. In fact, as postulated by the PM, in the endurance limit condition the local stress range,  $\Delta\sigma_y$ , equals the un-notched endurance limit at a distance from the notch tip equal to  $L/2$ ,  $L$  being in this case the unknown variable of the problem.

To conclude, it is worth observing that, in what follows, the accuracy of the TCD in estimating the high-cycle fatigue strength of notched plain concretes will be checked by estimating  $L$  according to the simplified strategy summarised in Figure 2e.

#### **4. Fundamentals of Gradient Elasticity**

In essence, the TCD is an extension of standard continuum mechanics whereby the results of linear elasticity are post-processed in order to arrive at a single stress measure that can be used to assess fatigue behaviour. As it turns out, this philosophy bears many similarities with the theory of gradient elasticity, whereby the standard equations of classical linear elasticity are expanded with additional, higher-order spatial derivatives of the relevant state variables. Analogous to the TCD, the theory of gradient of elasticity is equipped with one or more intrinsic length scales.

Enriching the continuum equations of elasticity with higher-order derivative terms has been explored systematically since the 19<sup>th</sup> century, see [25] for an overview. The mathematical structure of many of these different gradient elasticity theories means that their applicability to engineering problems is often hampered by a lack of available finite element implementations. However, the main exception is the gradient elasticity theory due to Aifantis of the early 1990s [26, 27]. The robustness and simplicity of the Aifantis theory relies in the fact that it includes only one length scale and that its format enables to write the governing equations as a sequence of two sets of partial differential equations. Namely, first the equations of classical elasticity are solved:

$$C_{ijkl}u_{k,jl} + b_i = 0 \quad (12)$$

where  $C_{ijkl}$  is a fourth-order tensor containing the elastic moduli,  $u_i$  are the displacements and  $b_i$  are the body forces. Equation (12) is solved together with the usual boundary conditions in terms of prescribed displacements and prescribed tractions, by which the displacements can be found. Next, these displacements are used as a source term in a second set of partial differential equations, that is

$$\sigma_{ij}^g - \ell^2 \sigma_{ij,mm}^g = C_{ijkl}u_{k,l} \quad (13)$$

from which an enriched stress field  $\sigma_{ij}^g$  can be found (the superscript  $g$  indicates that these stresses are gradient-enriched). The higher-order gradient term in Eq. (13) is accompanied by the (square of the) gradient elasticity length scale  $\ell$  which is introduced to capture the microstructural effects of the material – see [25] for a recent overview of interpretations and quantifications of the gradient elasticity length scale.

As noted above, one of the most attractive features of the Aifantis theory is the ease with which finite element implementations can be devised. Obviously, Eq. (12) leads to the

standard finite element equations of linear elasticity, but also the finite element discretisation of Eq. (13) is straightforward [26, 28, 29].

## 5. Experimental details

In order to check the accuracy of both the TCD and GE in estimating high-cycle fatigue strength of notched plain concrete, a systematic experimental investigation was carried out by testing, under cyclic four-point bending, square section beams containing three different geometrical features. The technical drawings reported in Figure 3 show the nominal dimensions of the tested specimens. The length of the beams was equal to 500 mm, the sides of the square cross sections had length equal to 100 mm, and the notch depth was equal to 50 mm. The three types of investigated notches had root radius equal to 25 mm (Fig. 3b), 12.5 mm (Fig. 3c), and 1.4 mm (Fig. 3d), resulting in a net stress concentration factor,  $K_t$ , of 1.47, 1.84, and 4.32, respectively. The geometry of the un-notched specimens is shown in Figure 3a. These samples were designed so that, during four-point bending testing, the portion of material subjected to a cyclic uniform bending moment had the same net width (i.e., 50 mm) as the notched specimens. By so doing, the generated results were not affected by the size effect, this holding true independently from the geometry of the specimens being tested.

To manufacture the samples sketched in Figure 3, the concrete mix was designed [30] using PFA Portland Cement with strength class equal to 32.5 N/mm<sup>2</sup>, natural round gravel with 10mm grading, and grade M concrete sand (cement content = 450 kg/m<sup>3</sup>; fine aggregate content = 825 kg/m<sup>3</sup>; coarse aggregate content = 825 kg/m<sup>3</sup>). Two different water-to-cement (w/c) ratios were chosen in order to cast specimens having the same material morphology with different strengths. In particular, Batch A was manufactured by setting the w/c ratio equal to 0.5, whereas Batch B had w/c ratio equal to 0.4. Following the ASTM recommendations [31], all the samples were removed from the moulds 24 hours after casting, being subsequently cured in a moist room at 23°C for 28 days. Both the un-notched

samples and the notched specimens with notch root radius equal to 25 mm and 12.5 mm were manufactured by casting the required geometrical features into the bulk material through plastic inserts directly attached to the bottom of the moulds. The sharp notches instead were machined by using a circular saw having thickness equal to 2.8 mm.

The pictures reported in Figure 4 show two examples of the macroscopic morphology of the investigated concrete from Batch A and Batch B, respectively, the average inter-aggregate distance being equal to about 4mm.

The static properties were determined under three-point bending as the average from five different tests per batch resulting in a flexural strength,  $f_B$ , equal to 4.9 MPa for Batch A and to 6.5 MPa for Batch B.

The fatigue results were generated by using a bespoke electric testing table which was modified and developed for this specific experimental investigation (Fig. 3e). The load histories applied during testing were gathered and recorded through two independent loading cells, the deflection at the mid-section of the samples being monitored via a linear LVDT. The adopted failure criterion was the complete breakage of the specimens. The force-controlled experiments were run at room temperature at a frequency of 10 Hz, the run out tests being stopped at  $2 \cdot 10^6$  cycles.

The results generated by testing under cyclic bending the specimens from Batch A and Batch B are summarised in Table 1 and 2, respectively. These tables report the code of the specimens, the measured width,  $w$ , and depth,  $d$ , of the net cross sectional area (see Figure 3), the notch root radius,  $r_n$ , the maximum nominal net stress in the cycle during testing,  $\sigma_{max}$ , the applied load ratio,  $R$ , and the experimental number of cycles to failure,  $N_f$ .

The pictures of Figure 5 show some examples of the fatigue cracking behaviour displayed by the investigated concrete. A close inspection of the fracture surfaces revealed that the fatigue cracks initiated mainly at the interfaces between matrix and aggregates, with the subsequent propagation occurring in the cement paste. The formation of relatively short fatigue cracks was followed by a fast fracture process leading to the complete failure of the samples. In

several cases, the final fast cracking resulted in the breakage of a few aggregates positioned away from the notch tip. According to the observed cracking behaviour, it is possible to conclude that, in the highly stressed region, the cement paste played the role of the weakest link in the fatigue strength of the microstructural chain, the interfaces between matrix and aggregate being the preferential crack initiation locations.

Following the same strategy as the one adopted in Ref. [1] to investigate the fatigue behaviour of un-notched plain and short fibre/particle reinforced concrete, the reference number of cycles to failure,  $N_o$ , for the determination of the endurance limits was taken equal to  $2 \cdot 10^6$  cycles to failure.

In order to determine the required endurance limits, the experimental data summarised in Tables 1 and 2 were generated according to Dixon's up-and-down procedure [32]. In particular, to apply this method, initially a tentative endurance limit has to be assumed, the first fatigue test being run at a stress level higher than the estimated value. If the specimen fails at reference number of cycles to failure lower than  $N_o$ , the subsequent test has to be run at a lower stress level. On the contrary, if the specimen lasts up to a number of cycles equal to  $N_o$ , then the following test has to be run at a higher stress level. By so doing, the stress level characterising each test depends on the previous experimental results, such a procedure being applied iteratively by increasing or decreasing the magnitude of the applied cyclic loading.

For each data set, the endurance limit for  $P_s=50\%$  was estimated from the experiments according to the following formula:

$$\sigma_{MAX} = \sigma_{LT} + K \cdot \delta \quad (14)$$

In Eq. (14)  $\sigma_{MAX}$  is the maximum nominal net stress in the fatigue cycle at the endurance limit,  $\delta$  is the interval between two adjacent stress levels and  $\sigma_{LT}$  is last test run for any material/geometry configuration. Lastly,  $K$  is a constant which can directly be extracted from

the table supplied by Dixon himself in Ref. [32] and compiled by performing a rigorous statistical analysis. To conclude, Figure 6 shows the Dixon diagrams built by post-processing the experimental tests listed in Tables 1 and 2, the results of such an analysis being concisely summarised also in Table 3. Both in Figure 4 and in Table 3  $R_m$  is the average value of the nominal load ratio,  $R$ , for each data set.

## **6. Validation by experimental data**

To investigate the reliability of microstructural length scale parameters in modelling the high-cycle fatigue behaviour of notched plain concrete, the TCD and GE have been applied by exploring bespoke strategies. The proposed reformulations for these two approaches are discussed in detail in the following sub-sections, their accuracy being checked against the notch endurance limits summarised in Table 3.

### **6.1. Preliminary considerations**

The common feature characterising the different formalisations of the TCD is that the extent of damage is quantified via an effective stress whose value depends not only on the magnitude of the local linear-elastic stress fields, but also on material length scale parameter  $L$ . In this context, critical distance  $L$  is treated as a material property whose value is not affected by the profile of the stress concentrator being assessed [11, 19]. Much experimental evidence shows that length  $L$  can be related to the material features at either a micro-, meso- or macro-scope level [11, 19], this depending on the morphological characteristics of the material being assessed as well as on the nature of the mechanisms resulting in the initiation and propagation of cracks. Similarly, GE length scale parameter  $l$  represents the underlying microstructure, its value being directly related to the size of the dominant source of microstructural heterogeneity [33]. Accordingly, under high-cycle fatigue loading, both  $L$  and  $l$  can range from a few microns [34, 35] up to several millimetres [11, 36].

Turning to the concrete mixes considered in the present investigation, as mentioned earlier, fatigue cracks were seen to initiate mainly due to the de-bonding phenomena occurring at the interfaces between cement paste and gravel, with the subsequent propagation process taking place in the matrix. Since the cement paste (at a mesoscopic scale) represents the weakest link in the structural chain of the investigated mixes,  $L$  and  $l$  are expected to have length of the order of the average inter-aggregate distance. This means that both the TCD and GE will be used to model the high-cycle fatigue behaviour of notched concrete by employing length scale parameters determined at a mesoscopic level. This aspect is very important since the investigated mixes had different water to cement ratios, this resulting in cement pastes characterised by different microstructural features.

As far as ductile materials are concerned, both the TCD and GE are seen to be capable of accommodating any material non-linearities into a linear-elastic constitutive law [11, 19, 35-37]. In particular, via length  $L$ , the magnitude of the effective stress used by the TCD to evaluate the extent of damage is reduced compared to that of the linear-elastic stress field close to the apex of the geometrical feature being assessed (see Figs 2c and 2d). Similarly, giving the boundary conditions, the use of GE leads to linear-elastic stress fields having, in the vicinity of the stress raiser apices being assessed, magnitude lower than the one of the corresponding stress fields determined according to classic continuum mechanics. As far as ductile materials are concerned, this allows the TCD and GE to mimic the smoothing effect of plasticity on the local stress fields without missing the undoubted advantages of linear stress/strain analyses. In notched/cracked ductile materials in the endurance limit condition the magnitude of the cyclic nominal loading is relatively small, so that the amount of material experiencing large scale plastic deformations is usually very limited [19]. Accordingly, local plasticity can be neglected with little loss of accuracy [11]. This should explain why the linear-elastic TCD as well as linear-elastic GE were seen to be capable of accurately predicting the high-cycle fatigue strength of cracked [18, 35-37], notched [18, 24, 36-39] and welded ductile metals [40-46].

Concrete is a quasi-brittle material whose mechanical behaviour displays different types of non-linearities, the physical processes resulting in such non-linearities being influenced mainly by the microstructural features of the mix. Owing to their accuracy in modelling the high-cycle fatigue behaviour of ductile materials, both the TCD and GE are expected to be capable of accommodating those local non-linearities characterising the mechanical behaviour of concrete into a simple linear-elastic framework. Thus, in what follows these two approaches will be applied by assuming that the stress vs. strain response of the assessed concrete mixes can effectively be modelled at a mesoscopic level via a simple linear-elastic constitutive law.

It is worth observing here also that the use of the TCD and GE to model the high-cycle fatigue behaviour of notched concrete is based on the assumption that  $L$  and  $l$  are independent parameters whose value is related solely to the material morphology. According to this assumption, the required length scale parameters can be defined without addressing the fracture energy problem *a priori*.

Much experimental evidence suggests that the frequency of the applied loading has a quite limited effect up to about 20Hz [47]. Accordingly, it is possible to presume that lengths  $L$  and  $l$  as well are not influenced by the frequency of the applied loading as long as the frequency itself does not affect the overall fatigue strength of the concrete being investigated. On the contrary, owing to the viscous behaviour characterising the mechanical behaviour of concrete, frequency is expected to become more and more important as the rate of the cyclic loading increases, this possibly affecting not only the strength of the investigated concrete, but also the related length scale parameters [48]. As mentioned in Section 5, the experimental results used to assess the accuracy of both the TCD and GE were generated at a frequency of 10Hz. Therefore, owing to the fact that the applied frequency was lower than 20Hz [47], the hypothesis was formed that its effect could be neglected with little loss of accuracy. However, in light of the complexity of this problem, it is evident that more

theoretical and experimental work needs to be done in this area in order to accurately study the frequency effect in concrete fatigue, this being out of the scopes of the present study.

## 6.2. Finite Element analyses

In order to apply the TCD, the continuum mechanics linear-elastic stress fields ahead of the investigated notches were determined by using commercial Finite Element (FE) software ANSYS®. The tested concrete was modelled as a homogenous and isotropic material. The notched beams were meshed using 2D element Plane 183, an 8-node element with quadratic displacement behaviour. The required linear elastic stress-distance curves were obtained by gradually increasing the mesh density in the notch tip regions until convergence occurred.

The GE FE models were solved by using an in-house finite element code developed at the Department of Civil and Structural Engineering of the University of Sheffield, UK. Both the un-notched and notched specimens were modelled by using quadrilateral four-noded bilinear elements. Also in this case, the mesh density in the regions of interest was gradually refined until convergence occurred. Finally, the numerical solutions were calculated by taking the boundary conditions of the gradient enrichment step of Eq. (13) as homogeneous natural boundary conditions throughout.

## 6.3. Theory of Critical Distances

Since the maximum stress in the cycle allows the mean stress effect in concrete fatigue to be modelled effectively, the PM, LM, and AM were reformulated as follows:

$$\sigma_{\text{eff,max}} = \sigma_{y,\text{max}} \left( \theta = 0^\circ, r = \frac{L}{2} \right) \quad (15)$$

$$\sigma_{\text{eff,max}} = \frac{1}{2L} \int_0^{2L} \sigma_{y,\text{max}}(\theta = 0^\circ, r) dr \quad (16)$$

$$\sigma_{\text{eff,max}} = \frac{4}{\pi L^2} \int_0^{\pi/2} \int_0^L \sigma_{1,\text{max}}(\theta, r) \cdot r \cdot dr \cdot d\theta \quad (17)$$

In the above definitions,  $\sigma_{\text{eff,max}}$  is the maximum value of the effective stress, whereas  $\sigma_{y,\text{max}}$  and  $\sigma_{1,\text{max}}$  are the maximum values of local stress components  $\sigma_y$  and  $\sigma_1$ , respectively.

Given definitions (15), (16), and (17), according to the TCD philosophy [11, 19] a notched concrete component is in the endurance limit condition as long as the maximum effective stress,  $\sigma_{\text{eff,max}}$ , is lower than (or, at least, equal to) the maximum endurance limit of the un-notched material,  $\sigma_{o,\text{MAX}}$ .

In order to apply the TCD to estimate the notch endurance limits summarised in Table 3, the critical distance value,  $L$ , for the investigated concrete was determined by following the strategy schematically summarised in Figure 2e, the stress quantities of interest being obviously expressed in terms of maximum values. As shown in the charts of Figure 7, the use of  $\sigma_{o,\text{MAX}}$  and the linear-elastic stress-distance curve determined, in the endurance limit condition, from the sharply notched specimens led to a critical distance value,  $L$ , for Batch A and Batch B of 5.8 mm. Since the material mesoscopic morphology was the same for both batches (see Figure 4), this result strongly supports the idea that length scale parameter  $L$  depends solely on those morphological features affecting the overall strength of the material being assessed. In particular, as mentioned earlier, in the investigated concrete the initiation process was seen to take place mainly at the interfaces between matrix and aggregates, the subsequent propagation occurring in the cement paste. Accordingly, the value for critical distance  $L$  estimated via the simplified procedure summarised in Figure 2e resulted in a length approaching the average inter-aggregate distance of 4mm.

Turning to the accuracy of the different formalisation of the TCD, the stress-distance curves plotted, at the endurance limit, in the charts of Figure 7 prove that the PM was highly accurate in estimating the high-cycle fatigue strength of the beams containing both the blunt ( $K_t=1.47$ ) and the intermediate notches ( $K_t=1.84$ ). The error bands reported in Figure 7 were determined by defining the error as follows:

$$\text{Error} = \frac{\sigma_{\text{eff,max}} - \sigma_{0,\text{MAX}}}{\sigma_{0,\text{MAX}}} [\%] \quad (18)$$

According to the above definition, an error larger than zero denotes a conservative prediction, whereas a negative error indicates a non-conservative estimate.

Table 4 confirms that the TCD used in the form of the PM and AM was capable of estimates falling within an error interval of about  $\pm 10\%$  independently of the sharpness of the assessed notch. On the contrary, the predictions made using the LM were seen to fall on the non-conservative side, within an error interval of about  $\pm 20\%$ .

To conclude, it can be noticed that the obtained level of accuracy is certainly encouraging since, as far as notches are concerned, it is not possible to distinguish between an error of  $\pm 20\%$  and an error of  $0\%$  as a consequence of those problems that are usually encountered when performing the testing as well as the numerical analyses [49].

#### **6.4. Gradient elasticity applied according to the Theory of Critical Distances**

In two recent investigations [37, 50], it has been proven that gradient-enriched crack tip stresses are capable of accurately modelling, at the threshold condition, the transition from the long- to the short-crack regime, both under high-cycle fatigue [37] and static loading [50]. Due to the high level of accuracy that was obtained by following such a strategy, in the present investigation as well the hypothesis is formed that the high-cycle fatigue strength of notched plain concrete can directly be estimated through the linear-elastic gradient-enriched stress state determined at the notch tip. Further, as discussed in Section 2, GE has to be applied in terms of maximum values of the stresses in the fatigue cycle in order to efficiently take into account the mean stress effect in concrete fatigue. According to the above considerations, the maximum value of the GE effective stress is suggested here as being calculated as follows (see also Fig. 2a):

$$\sigma_{\text{eff,max}} = \sigma_{y,\text{max}}(\theta = 0^\circ, r = 0) \quad (19)$$

where, in this case,  $\sigma_{y,\text{max}}$  denotes the gradient-enriched stress perpendicular to axis x (see Figure 2a for the definition of the local frame of reference). Therefore, similar to the TCD, the assumption can be made that the notched concrete being designed is at its endurance limit (i.e., in the threshold condition) when  $\sigma_{\text{eff,max}}$  equals the maximum endurance limit of the un-notched material,  $\sigma_{o,\text{MAX}}$ .

The second information which is needed to calculate the effective stress via definition (19) is microstructural length scale parameter  $l$ . By following a reasoning based on non-local mechanics, it was proven in Ref. [37] that  $l$  can directly be estimated from the TCD critical distance value,  $L$ , via the following relationship:

$$l = \frac{L}{2\sqrt{2}} \quad (20)$$

Therefore, GE was applied in accordance with the TCD to estimate the notch endurance limits of the tested concrete by taking the length scale parameter,  $l$ , equal to 2.05 mm,  $L$  being equal to 5.8 mm. The diagrams reported in Figure 8 show the gradient-enriched stress fields determined, at the endurance limit, for  $l=2.05$  mm, the error being calculated via definition (18). These diagrams together with Table 4 make it evident that the use of GE applied according to the TCD resulted in conservative estimates, the level of conservatism increasing with the increase of the notch sharpness.

To conclude, since  $L$  can easily be derived either via definition (8) re-arranged in terms of maximum values or through the simplified procedure summarised in Figure 2e, the obtained results strongly support the idea that GE can safely be used in conjunction with the TCD's philosophy by always reaching during the design process an appropriate level of safety.

#### **6.4. Gradient elasticity and material microstructural features**

By carefully observing the diagrams of Figure 8, it is possible to notice that, in the endurance limit condition, the gradient-enriched stress at the surface of the un-notched specimens is lower than the corresponding endurance limit determined according to continuum mechanics. This situation is schematically shown also in Figure 9a where  $\sigma_{\text{GEO,max}}$  is used to denote the maximum value of the endurance limit determined via GE. This apparent anomaly is a consequence of the fact that, in the presence of stress gradients, GE manipulates the local stress fields by incorporating into the stress analysis the microstructural length scale parameter,  $\ell$ . Solely in the absence of gradients the stress fields determined via GE coincide with those determined according to continuum mechanics. This is what happens, for instance, under axial loading - see Figure 9b where  $\sigma_{\text{GEO,MAX}} = \sigma_{\text{o,MAX}}$ . Therefore, one may argue that the conventional un-notched endurance limit,  $\sigma_{\text{o,MAX}}$ , determined under bending is not a strength quantity suitable for being used to employ GE to estimate the high-cycle fatigue strength of notched materials. Having said that, the hypothesis can be formed that  $\sigma_{\text{GEO,MAX}}$  can directly be derived from the experimental results generated by testing un-notched specimens under cyclic bending provided that the value of the length scale parameter,  $\ell$ , is set *a priori*. In order to choose an appropriate value for the microstructural length scale parameter, it is worth remembering here that length  $\ell$  is seen to be directly related to the size of the dominant source of microstructural heterogeneity [33]. Therefore, the assumption can be made that  $\ell$  equals the average inter-aggregate distance, i.e.,  $\ell = 4$  mm, since in the tested concrete the cement paste was seen to play the role of the weakest link in the fatigue strength of the microstructural chain (Fig. 5). As shown in the diagrams of Figures 10a and 10b, taking the length scale parameter equal to 4 mm resulted in a maximum value of the GE un-notched endurance limit,  $\sigma_{\text{GEO,MAX}}$ , equal to 2.8 MPa for Batch A and to 4.3 MPa for Batch B. The gradient-enriched stress-distance curves reported in the above charts make it evident that the use of such a strategy resulted in highly accurate

predictions, with estimates falling within an error interval of  $\pm 10\%$  (see Table 4). To conclude, it is worth observing that in Figures 9c and 9d as well as in Table 4 the error was calculated as follows:

$$\text{Error} = \frac{\sigma_{\text{eff,max}} - \sigma_{\text{GE0,MAX}}}{\sigma_{\text{GE0,MAX}}} [\%] \quad (21)$$

where  $\sigma_{\text{eff,max}}$  was determined according to definition (19).

## 7. Conclusions

In the present paper the accuracy and reliability of microstructural length scale parameters in modelling the high-cycle fatigue behaviour of notched plain concrete was checked against an appropriate set of experimental data. The most important conclusions can be summarised as follows:

- the maximum stress in the cycle is seen to be capable of modelling the mean stress effect in concrete fatigue also in the presence of notches;
- the use of both the PM and AM resulted in highly accurate estimates, this proving that these two formalisations of the TCD are suitable for modelling the high-cycle fatigue behaviour of notched plain concrete;
- even though the obtained error level was acceptable, the use of the LM led to non-conservative estimates;
- the fact that the TCD critical distance was seen to be the same in both batches strongly supports the idea that  $L$  mainly depends on the material microstructural features;
- the use of GE applied according to the TCD resulted in conservative estimates, the level of conservatism increasing with the sharpness of the notch;

- GE applied by taking length scale parameter  $l$  equal to the average inter-aggregate distance was seen to result in a remarkable level of accuracy. This strongly supports the idea that length  $l$  is a parameter suitable for modelling the dominant source of microstructural heterogeneity;
- more work needs to be done in this area to check the accuracy of the TCD and GE not only with other plain and short-fibre reinforced concrete containing different notches, but also under mixed mode loading.

## References

- [1] Susmel L. A unifying methodology to design un-notched plain and short-fibre/particle reinforced concretes against fatigue. *Int J Fatigue* 2014;61:226–243.
- [2] Anon. Nuclear Construction Lesson Learned – Guidance on best practice: concrete. The Royal Academy of Engineering, London, 2012. ISBN: 1-903496-81-0.
- [3] Ohlsson U, Daerga PA, Elfgren L. Fracture energy and fatigue strength of unreinforced concrete beams at normal and low temperatures. *Engng Frac Mech* 1990;35 1/2/3:195-203.
- [4] Plizzari GA, Cangiano S, Alleruzzo S. The fatigue behaviour of cracked concrete. *Fatigue Fract Engng Mater Struct* 1997; 20 8: 1195-1206.
- [5] Thun H, Ohlsson U, Elfgren L. A deformation criterion for fatigue of concrete in tension. *Structural Concrete* 2011;12 3:187-197.
- [6] Von Ornum JL. Fatigue of cement products. *ASCE Transactions* 1903;51:443-451.
- [7] Von Ornum JL. Fatigue of concrete. *ASCE Transactions* 1907;58:294-320.
- [8] Zhang B. Relationship Between Pore Structure and Mechanical Properties of Ordinary Concrete Under Bending Fatigue. *Cem Concr Res* 1998;28 5:699–711.
- [9] Guo L-P, Sun W, Zheng K-R, Chen H-J, Liu B. Study on the flexural fatigue performance and fractal mechanism of concrete with high proportions of ground granulated blast-furnace slag. *Cem Concr Res* 2007;37 2:242–250.
- [10] Murdock J, Kesler CE. The Mechanism of Fatigue in Concrete. Report No. 587, University of Illinois, August 1960.
- [11] Susmel L. *Multiaxial Notch Fatigue: from nominal to local stress-strain quantities*. Woodhead & CRC, Cambridge, UK, ISBN: 1 84569 582 8, March 2009.
- [12] Spindel JE, Haibach E. Some considerations in the statistical determination of the shape of S-N curves. In: *Statistical Analysis of Fatigue Data*, ASTM STP 744, Edited by Little RE and Ekvall JC 1981:89–113.
- [13] Hobbacher A. Recommendations for fatigue design of welded joints and components. IIW document XIII-2151-07/XV-1254-07; May 2007.
- [14] Anon. ENV 1993-1-1, EUROCODE 3 – Design of steel structures, 1988.
- [15] Haibach E. *Service fatigue-strength – methods and data for structural analysis*. VDI, Düsseldorf, Germany, 1992.

- [16] Neuber H. *Theory of notch stresses: principles for exact calculation of strength with reference to structural form and material*. Springer Verlag, Berlin, II Edition, 1958.
- [17] Peterson RE. Notch Sensitivity. In: *Metal Fatigue*, Edited by G. Sines and J. L. Waisman, McGraw Hill, New York, pp. 293-306, 1959.
- [18] Taylor D. Geometrical effects in fatigue: a unifying theoretical model. *Int J Fatigue* 1999;21:413-420.
- [19] Taylor D. *The Theory of Critical Distances: A New Perspective in Fracture Mechanics*. Elsevier Science, Cambridge, UK, 2007.
- [20] Bellett D, Taylor D, Marco S, Mazzeo E, Guillois J, Pircher T. The fatigue behaviour of three-dimensional stress concentrations. *Int J Fatigue* 2005; 27:207-221.
- [21] El Haddad MH, Topper TH, Smith KN. Prediction of non-propagating cracks. *Engng Frac Mech* 1979;11:573-584.
- [22] Karihaloo BL. *Fracture Mechanics and Structural Concrete*. Longman Scientific & Technical, London, UK, 1995.
- [23] Susmel L. A unifying approach to estimate the high-cycle fatigue strength of notched components subjected to both uniaxial and multiaxial cyclic loadings. *Fatigue Fract Engng Mater Struct* 2004;27:391-411.
- [24] Susmel L, Taylor D. A novel formulation of the Theory of Critical Distances to estimate Lifetime of Notched Components in the Medium-Cycle Fatigue Regime. *Fatigue Fract Engng Mater Struct* 2007;30 7:567-581.
- [25] Askes H, Aifantis EC. Gradient elasticity in statics and dynamics: An overview of formulations, length scale identification procedures, finite element implementations and new results. *Int J Solids Struct* 2011;48:1962-1990.
- [26] Aifantis EC. On the role of gradients in the localization of deformation and fracture. *Int J Engng Sci* 1992;30:1279-1299.
- [27] Ru CQ, Aifantis EC, A simple approach to solve boundary-value problems in gradient elasticity. *Acta Mech* 1993;101:59-68
- [28] Tenek LT, Aifantis EC. A two-dimensional finite element implementation of a special form of gradient elasticity. *Comput Model Engng Sci* 2002;3:731-741.
- [29] Askes H, Morata I, Aifantis E.C. Finite element analysis with staggered gradient elasticity. *Comput Struct* 2008;86:1266-1279.
- [30] Teychenne DC, Franklin RE, Erntroy HC, Hobbs DW, Marsh BK. *Design of Normal Concrete Mixes*. Construction Research Communications, 2<sup>nd</sup> Edition, 2010. ISBN-13: 978-1860811722.
- [31] ASTM Standard C192/C192M, Standard Practice for Making and Curing Concrete Test Specimens in the Laboratory, ASTM International, West Conshohocken PA, 2007.
- [32] Dixon WJ. The up-and-down method for small samples. *Journal of the American Statistical Association* 1965;60 312:967-978.
- [33] Gitman IM, Askes H, Aifantis EC. The representative volume size in static and dynamic micro-macro transitions. *Int J Fract* 2005;135:L3-L9.
- [34] Wiersma S, Taylor D. Fatigue of materials used in microscopic components. *Fatigue Fract Engng Mater Struct* 2005;28 12:1153-1160.
- [35] Askes H, Susmel L. Understanding cracked materials: is Linear Elastic Fracture Mechanics obsolete? *Fatigue Fract Engng Mater Struct* 2015;38:154-160.

- [36] Askes H, Livieri P, Susmel L, Taylor D, Tovo R. Intrinsic material length, Theory of Critical Distances and Gradient Mechanics: analogies and differences in processing linear-elastic crack tip stress fields. *Fatigue Fract Engng Mater Struct* 2013;36:39–55.
- [37] Susmel L, Askes H, Bennett T, Taylor D. Theory of Critical Distances vs. Gradient Mechanics in modelling the transition from the short- to long-crack regime at the fatigue limit. *Fatigue Fract Engng Mater Struct* 2013;36:861-869, 2013.
- [38] Susmel L, Taylor D. Fatigue Design in the Presence of Stress Concentrations. *J Strain Anal Eng Des* 2003;38 5:443-452.
- [39] Susmel L. The Theory of Critical Distances: a review of its applications in fatigue. *Eng Frac Mech* 75, pp. 1706-1724, 2008.
- [40] Taylor D, Barrett N, Lucano G. Some new methods for predicting fatigue in welded joints. *Int J Fatigue* 2002;24 5:509-518.
- [41] Susmel L. Modified Wöhler Curve Method, Theory of Critical Distances and EUROCODE 3: a novel engineering procedure to predict the lifetime of steel welded joints subjected to both uniaxial and multiaxial fatigue loading. *Int J Fatigue* 2008;30:888-907.
- [42] Susmel L. The Modified Wöhler Curve Method calibrated by using standard fatigue curves and applied in conjunction with the Theory of Critical Distances to estimate fatigue lifetime of aluminium weldments. *Int J Fatigue* 2009;31:197-212.
- [43] Susmel L. Four stress analysis strategies to use the Modified Wöhler Curve Method to perform the fatigue assessment of weldments subjected to constant and variable amplitude multiaxial fatigue loading. *Int J Fatigue* 2014;64:38-54.
- [44] Tovo R, Livieri P. An implicit gradient application to fatigue of sharp notches and weldments. *Engng Frac Mech* 2007;74 4:515-526.
- [45] Livieri P, Tovo R. The effect of throat underflushing on the fatigue strength of fillet weldments. *Fatigue Fract Engng Mater Struct* 2013;36 9:884-892.
- [46] Livieri P, Tovo R. Numerical methods for calculating the structural reliability of fatigue-loaded welds. *Welding International* 2014;28 11:865-872.
- [47] Raithby KD. Flexural fatigue behaviour of plain concrete. *Fatigue Fract Engng Mater Struct* 1979;2:269-278.
- [48] Lee MK, Barr BIG. An overview of the fatigue behaviour of plain and fibre reinforced concrete. *Cement Concrete Comp* 2004;26:299–305.
- [49] Taylor, D., Wang, G. The validation of some methods of notch fatigue analysis. *Fatigue Fract Engng Mater Struct* 2000;23:387–394.
- [50] Askes, H., Susmel, L., Gradient enriched linear-elastic crack tip stresses to estimate the static strength of cracked engineering ceramics. *Frattura ed Integrità Strutturale* 2013;25:87-93.

## List of Captions

- Table 1.** Summary of the fatigue results generated by testing the specimens from Batch A.
- Table 2.** Summary of the fatigue results generated by testing the specimens from Batch B.
- Table 3.** Summary of the endurance limits determined, at  $N_0=2 \cdot 10^6$  cycles to failure, according to the up-and-down method.
- Table 4.** Overall accuracy obtained by using microstructural length scale parameters in estimating the high-cycle fatigue strength of the tested notched concrete.
- Figure 1.** Concrete beam loaded in cyclic bending (a) and subjected to cyclic axial loading (b); load histories characterised by different values of the load ratio (c, d); Wöhler diagram and fatigue curves for different values of  $P_s$  (e); unifying Wöhler diagram to perform the fatigue assessment of un-notched plain and short fibre/particle reinforced concretes (grey markers = run outs) [1] (f).
- Figure 2.** Notched component and local frame of reference (a); range of the effective stress,  $\Delta\sigma_{\text{eff}}$ , calculated according to the Area (b), Point (b), and Line Method (c); simplified experimental procedure to estimate critical distance  $L$  (e).
- Figure 3.** Geometry of the investigated specimens (dimensions in millimetres) and fatigue testing apparatus.
- Figure 4.** Macroscopic morphology of the tested concrete.
- Figure 5.** Macroscopic cracking behaviour under fatigue loading displayed by the tested concrete.
- Figure 6.** Endurance limits determined according to the up-and-down method.
- Figure 7.** Local linear-elastic stress fields in the endurance limit condition and accuracy of the PM in estimating the high-cycle fatigue strength of the tested notched concrete.
- Figure 8.** Gradient-enriched stress fields in the endurance limit condition and accuracy of GE applied according to the TCD in estimating the high-cycle fatigue strength of the tested notched concrete.
- Figure 9.** Continuum mechanics vs. gradient-enriched stress fields in a beam subjected to cyclic bending (a) as well as to cyclic axial loading (b); accuracy of GE calibrated via average the inter-aggregate distance in estimating the high-cycle fatigue strength of the tested notched concrete (c, d).

## Tables

<b>Code</b>	<b>d</b> [mm]	<b>w</b> [mm]	<b>r<sub>n</sub></b> [mm]	<b>σ<sub>max</sub></b> [MPa]	<b>R</b>	<b>N<sub>f</sub></b> [Cycles]	<b>Run Out</b>
P-A-1	101.6	53.1	-	3.4	0.16	132300	
P-A-2	101.6	52.9	-	3.2	0.11	2·10 <sup>6</sup>	•
P-A-3	99.6	53.4	-	3.4	0.09	175600	
P-A-4	99.6	53.2	-	3.2	0.06	1911600	
B-A-1	101.0	50.5	25.0	3.7	0.05	500	
B-A-2	101.3	49.6	25.0	3.5	0.05	3800	
B-A-3	100.0	50.0	25.0	3.3	0.06	2·10 <sup>6</sup>	•
B-A-4	101.4	51.0	25.0	3.5	0.10	1890800	
B-A-5	100.8	49.4	25.0	3.3	0.08	36600	
B-A-6	101.4	51.0	25.0	3.1	0.08	2·10 <sup>6</sup>	•
B-A-7	100.0	50.0	25.0	3.4	0.05	2·10 <sup>6</sup>	•
I-A-1	100.4	49.3	12.5	3.5	0.06	147100	
I-A-2	100.0	50.0	12.5	3.3	0.06	551000	
I-A-3	100.0	50.2	12.5	3.2	0.10	312900	
I-A-4	100.4	52.8	12.5	2.9	0.07	2·10 <sup>6</sup>	•
I-A-5	100.4	49.3	12.5	3.2	0.12	2·10 <sup>6</sup>	•
I-A-6	100.4	52.8	12.5	3.4	0.12	2·10 <sup>6</sup>	•
S-A-1	100.3	46.1	1.4	3.6	0.13	22200	
S-A-2	100.6	49.8	1.4	3.3	0.06	523600	
S-A-3	101.7	50.4	1.4	3.1	0.14	2·10 <sup>6</sup>	•
S-A-4	101.4	46.9	1.4	3.4	0.18	2·10 <sup>6</sup>	•
S-A-5	101.7	50.4	1.4	3.6	0.11	855200	
S-A-6	101.7	49.7	1.4	3.4	0.06	2·10 <sup>6</sup>	•

**Table 1.** Summary of the fatigue results generated by testing the specimens from Batch A.

<b>Code</b>	<b>d</b> [mm]	<b>w</b> [mm]	<b>r<sub>n</sub></b> [mm]	<b>σ<sub>max</sub></b> [MPa]	<b>R</b>	<b>N<sub>f</sub></b> [Cycles]	<b>Run Out</b>
P-B-1	101.4	49.0	-	5.0	0.31	2·10 <sup>6</sup>	•
P-B-2	100.6	49.3	-	5.4	0.37	700	
P-B-3	100.7	48.7	-	5.1	0.31	2·10 <sup>6</sup>	•
P-B-4	99.2	48.5	-	5.4	0.34	71500	
P-B-5	101.0	49.0	-	5.0	0.32	468900	
B-B-1	101.1	50.8	25.0	5.1	0.43	2600	
B-B-2	101.2	51.0	25.0	4.8	0.40	180200	
B-B-3	100.9	51.5	25.0	4.5	0.37	2·10 <sup>6</sup>	•
B-B-4	101.4	51.7	25.0	4.8	0.37	226300	
B-B-5	101.0	51.8	25.0	4.5	0.39	2·10 <sup>6</sup>	•
B-B-6	100.0	50.2	25.0	4.8	0.44	343200	
I-B-1	100.3	53.3	12.5	4.7	0.37	2·10 <sup>6</sup>	•
I-B-2	101.8	51.6	12.5	4.9	0.37	1070200	
I-B-3	100.8	52.3	12.5	4.7	0.36	225600	
I-B-4	101.0	47.0	12.5	4.5	0.32	2·10 <sup>6</sup>	•
I-B-5	100.2	51.0	12.5	4.7	0.32	159700	
I-B-6	101.0	48.8	12.5	4.5	0.33	3100	
S-B-1	101.0	51.2	1.4	4.5	0.37	2·10 <sup>6</sup>	•
S-B-2	101.0	49.2	1.4	4.7	0.34	1935400	
S-B-3	101.7	49.8	1.4	4.5	0.33	2·10 <sup>6</sup>	•
S-B-4	100.7	49.9	1.4	4.7	0.36	75200	
S-B-5	101.1	49.8	1.4	4.5	0.32	2·10 <sup>6</sup>	•

**Table 2.** Summary of the fatigue results generated by testing the specimens from Batch B.

<b>Batch</b>	<b>f<sub>b</sub></b> [MPa]	<b>N. of tests</b>	<b>r<sub>n</sub></b> [mm]	<b>K<sub>t</sub></b>	<b>R<sub>m</sub></b>	<b>δ</b>	<b>K</b>	<b>σ<sub>MAX</sub></b> [MPa]
A	4.9	4	-	1.00	0.11	0.20	0.299	3.3
		7	25	1.47	0.07	0.19	-0.144	3.1
		6	12.5	1.84	0.09	0.23	0.500	3.0
		6	1.4	4.36	0.11	0.22	-0.169	3.1
B	6.5	5	-	1.00	0.33	0.36	0.084	5.1
		6	25	1.47	0.40	0.25	0.737	4.7
		6	12.5	1.84	0.35	0.20	0.296	4.6
		5	1.4	4.36	0.34	0.20	0.701	4.6

**Table 3.** Summary of the endurance limits determined, at  $N_0=2 \cdot 10^6$  cycles to failure, according to the up-and-down method.

<b>K<sub>t</sub></b>	<b>Error [%]</b>									
	<b>Batch A</b>					<b>Batch B</b>				
	<b>PM</b>	<b>LM</b>	<b>AM</b>	<b>GE</b> ℓ=2.05mm	<b>GE</b> ℓ=4mm	<b>PM</b>	<b>LM</b>	<b>AM</b>	<b>GE</b> ℓ=2.05mm	<b>GE</b> ℓ=4mm
1.47	3.0	-18.7	5.7	11.2	8.2	1.0	-20.3	3.7	10.0	7.7
1.84	4.8	-20.0	9.3	19.7	8.6	4.0	-20.6	8.5	17.6	7.4
4.32	0.0	-13.1	10.8	29.4	-3.6	0.0	-16.5	6.3	25.5	-6.0

**Table 4.** Overall accuracy obtained by using microstructural length scale parameters in estimating the high-cycle fatigue strength of the tested notched concrete.

**Figures**

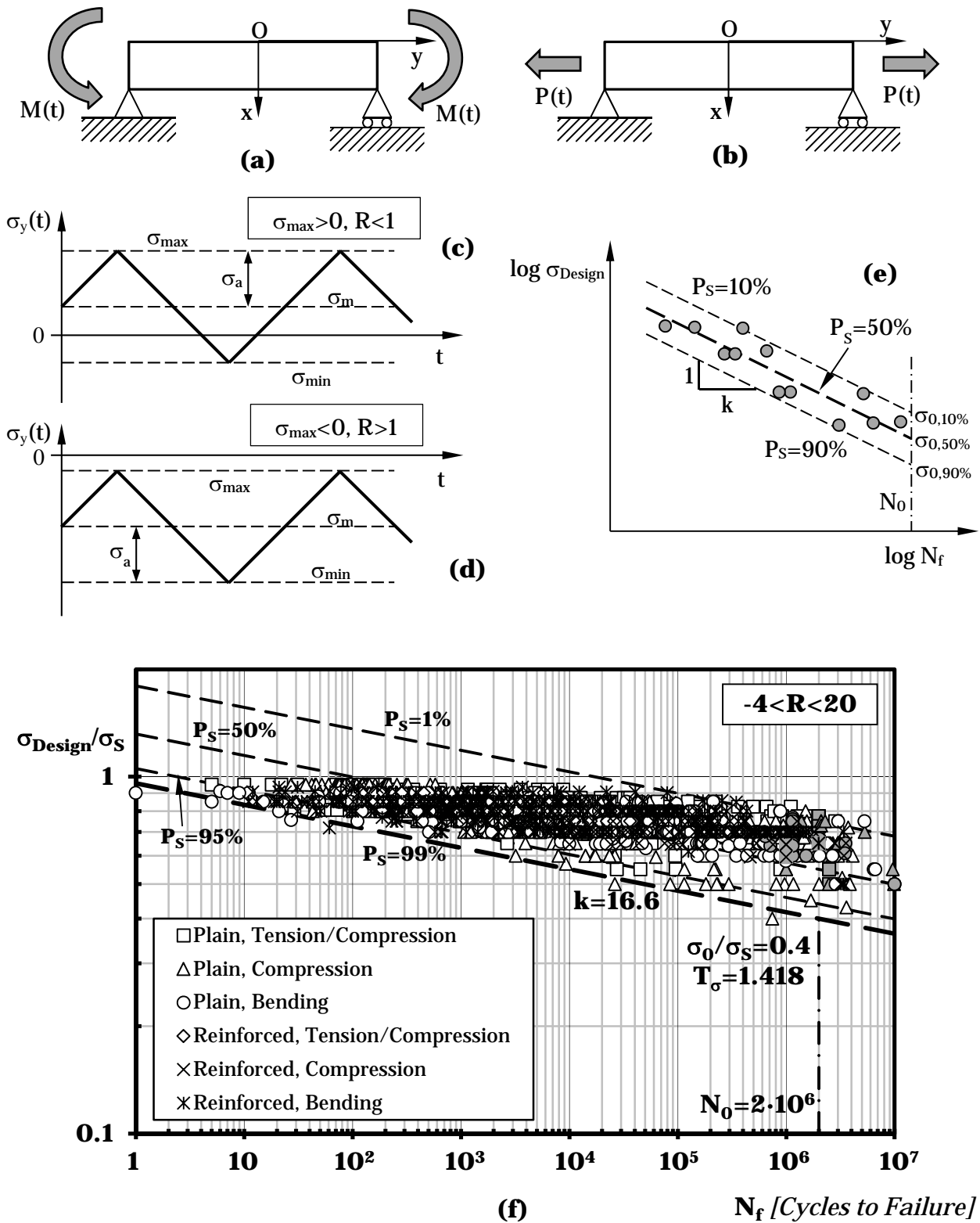


**Figure 1.** Concrete beam loaded in cyclic bending (a) and subjected to cyclic axial loading (b); load histories characterised by different values of the load ratio (c, d); Wöhler diagram and fatigue curves for different values of  $P_S$  (e); unifying Wöhler diagram to perform the fatigue assessment of un-notched plain and short fibre/particle reinforced concretes (grey markers = run outs) [1] (f).

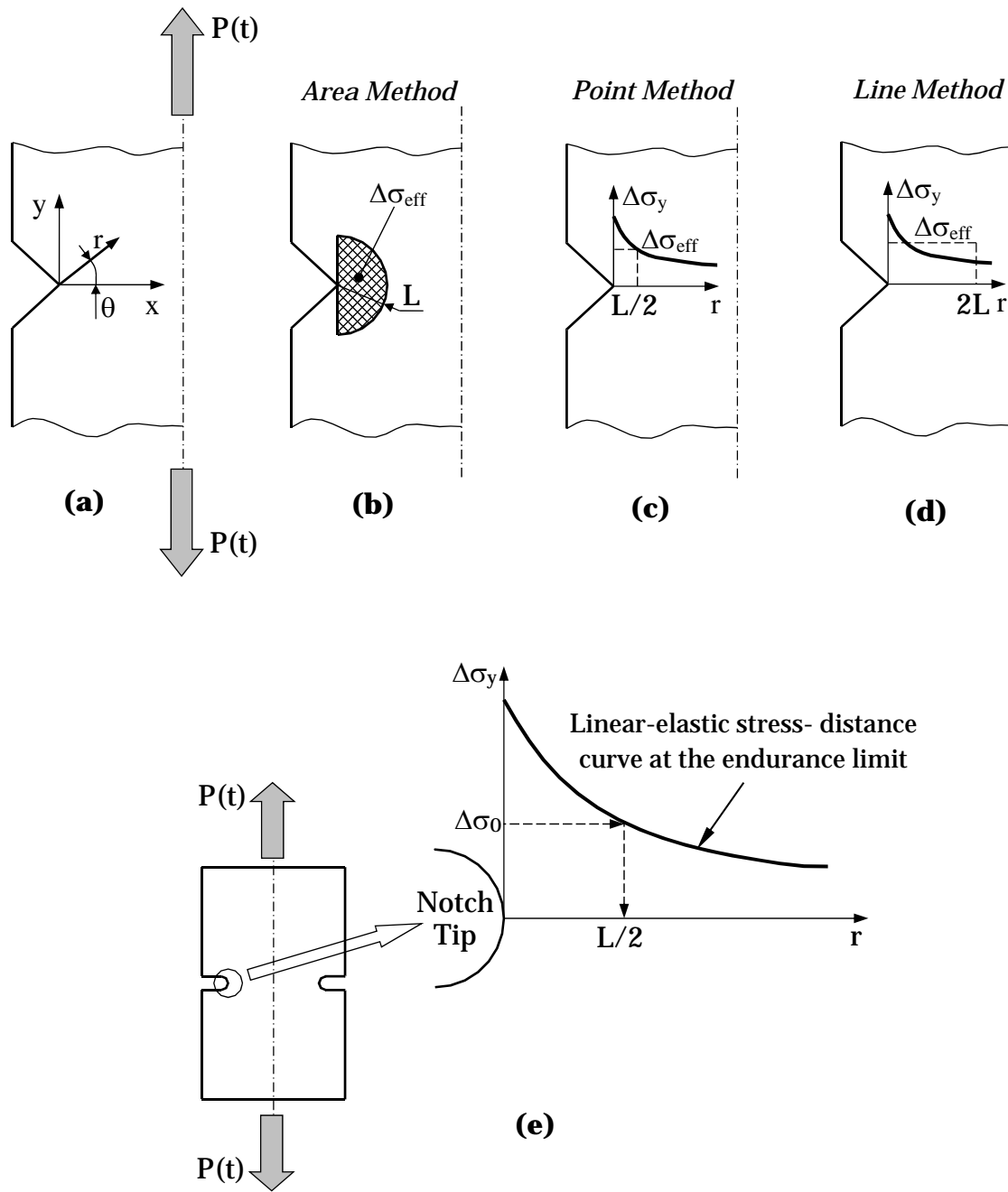


**Figure 2.** Notched component and local frame of reference (a); range of the effective stress,  $\Delta\sigma_{eff}$ , calculated according to the Area (b), Point (b), and Line Method (c); simplified experimental procedure to estimate critical distance  $L$  (e).

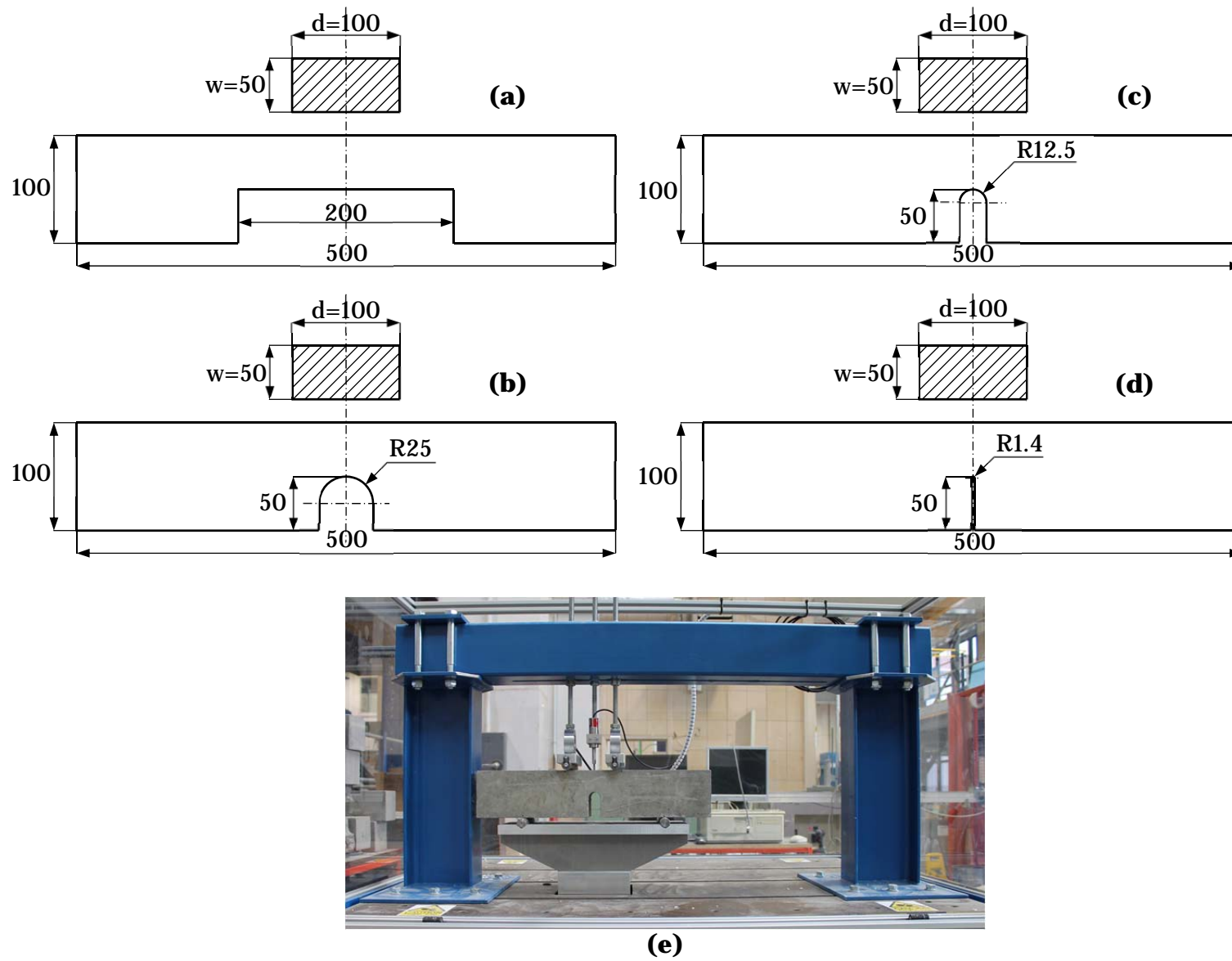
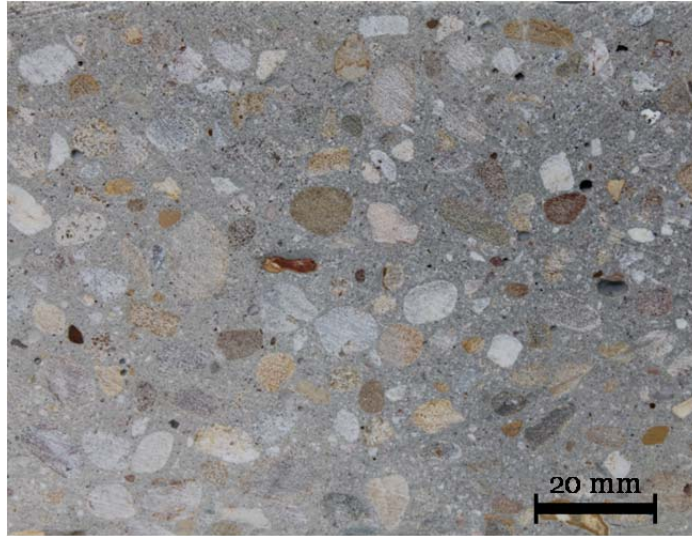


**Figure 3.** Geometry of the investigated specimens (dimensions in millimetres) and fatigue testing apparatus.



**Batch A**



**Batch B**

**Figure 4.** Macroscopic morphology of the tested concrete.

	$K_t=1$	$K_t=1.47$	$K_t=1.84$	$K_t=4.32$
Batch A	<p>P-A-3, <math>\sigma_{max}=3.4</math> MPa, R=0.09</p>  <p>Crack initiation surface</p>	<p>B-A-5, <math>\sigma_{max}=3.3</math> MPa, R=0.08</p>  <p>Notch Tip</p>	<p>I-A-1, <math>\sigma_{max}=3.5</math> MPa, R=0.06</p>  <p>Notch Tip</p>	<p>S-A-2, <math>\sigma_{max}=3.3</math> MPa, R=0.06</p>  <p>Notch Tip</p>
Batch B	<p>P-B-4, <math>\sigma_{max}=5.4</math> MPa, R=0.34</p>  <p>Crack initiation surface</p>	<p>B-B-4, <math>\sigma_{max}=4.8</math> MPa, R=0.37</p>  <p>Notch Tip</p>	<p>I-B-5, <math>\sigma_{max}=4.7</math> MPa, R=0.32</p>  <p>Notch Tip</p>	<p>S-B-2, <math>\sigma_{max}=4.7</math> MPa, R=0.34</p>  <p>Notch Tip</p>

**Figure 5.** Macroscopic cracking behaviour under fatigue loading displayed by the tested concrete.

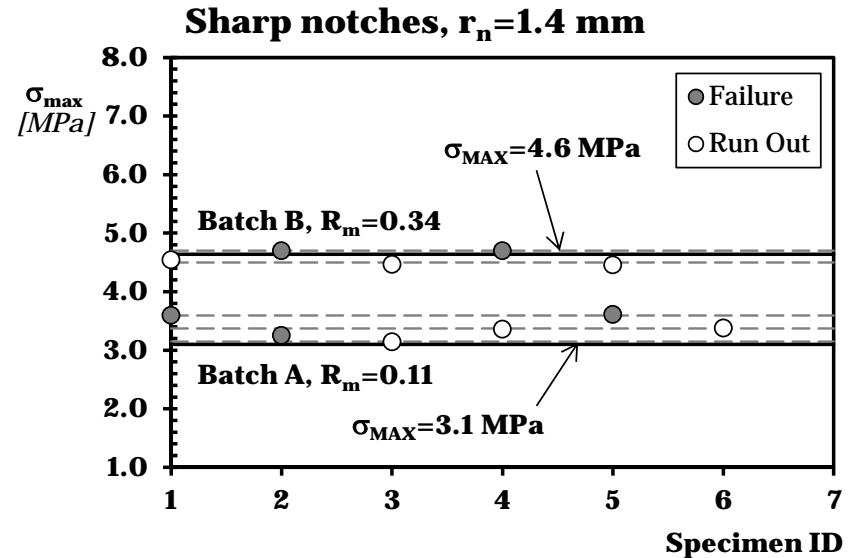
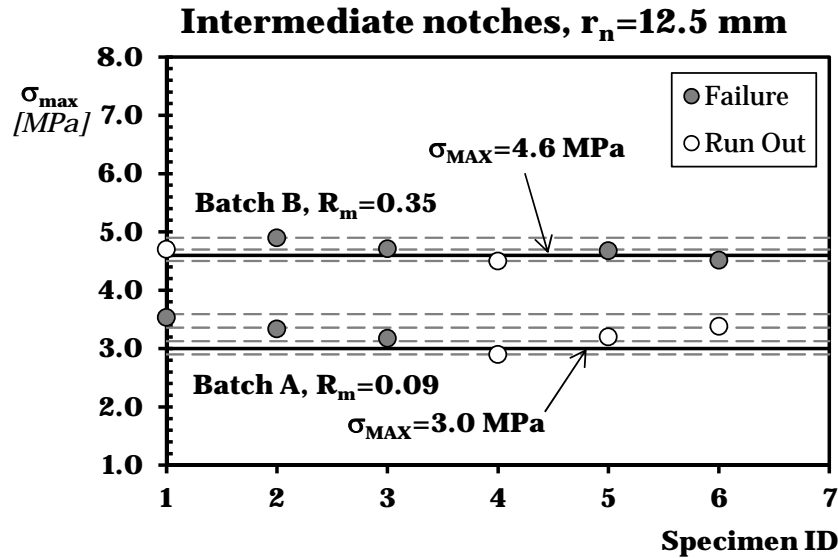
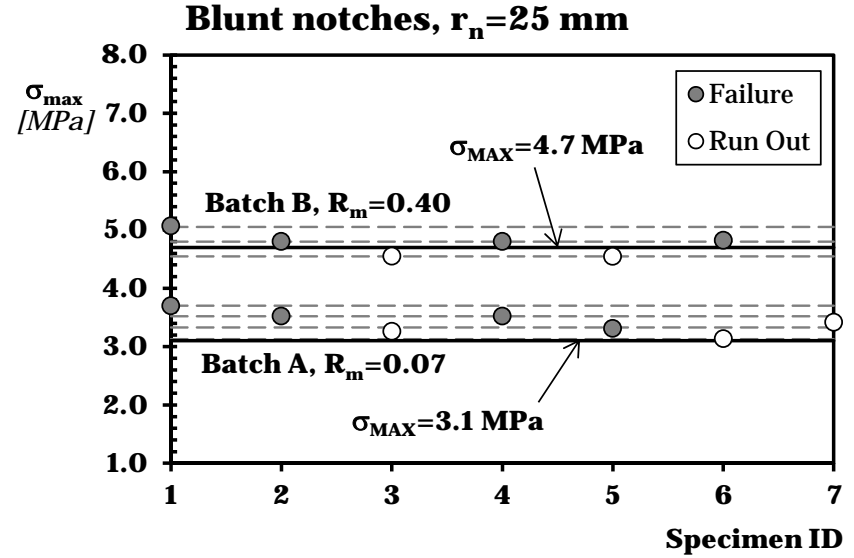
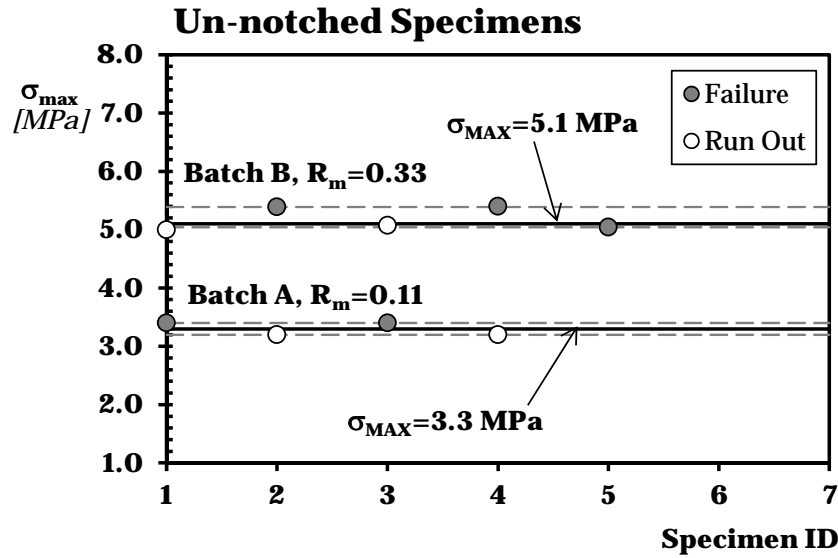


**Figure 6.** Endurance limits determined according to the up-and-down method.

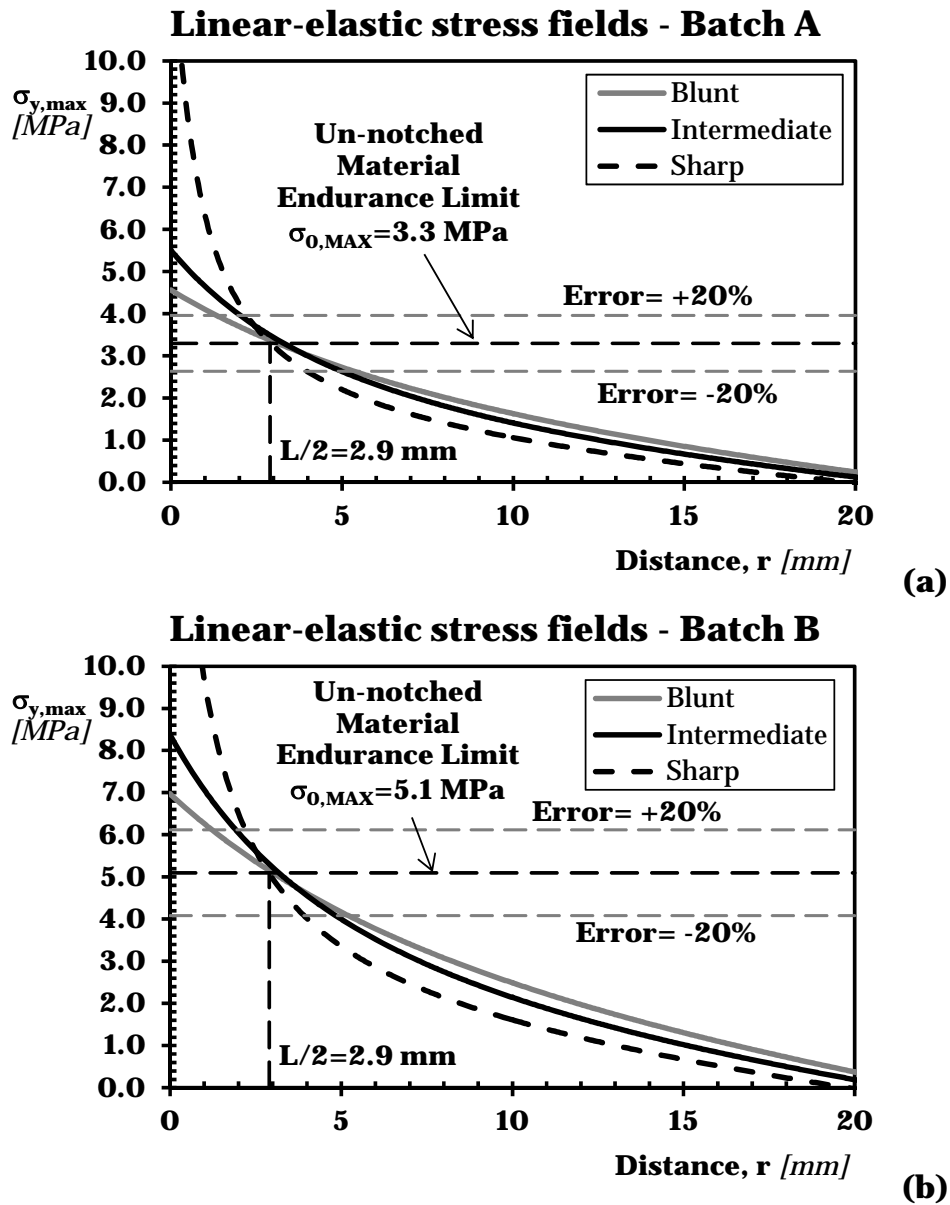


**Figure 7.** Local linear-elastic stress fields in the endurance limit condition and accuracy of the PM in estimating the high-cycle fatigue strength of the tested notched concrete.

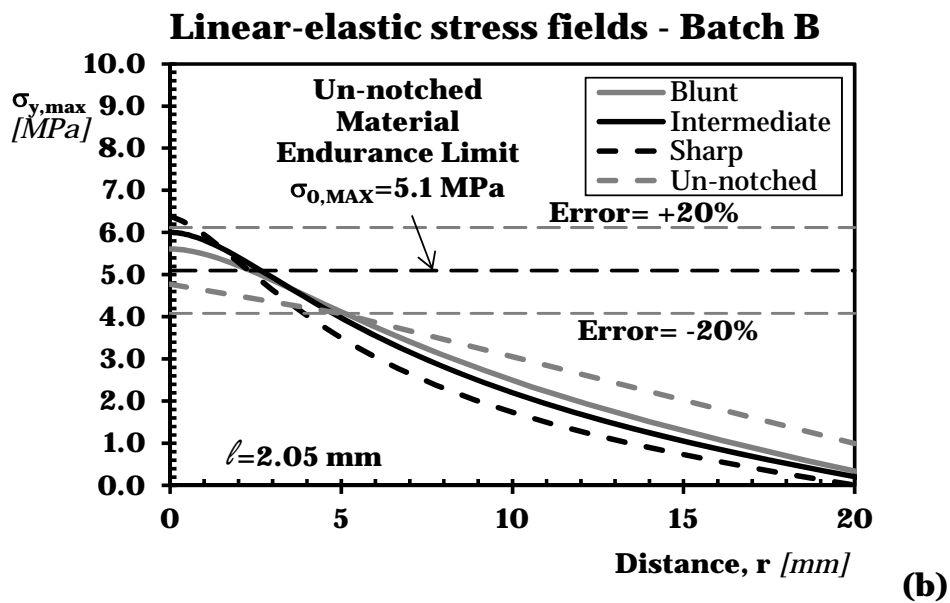
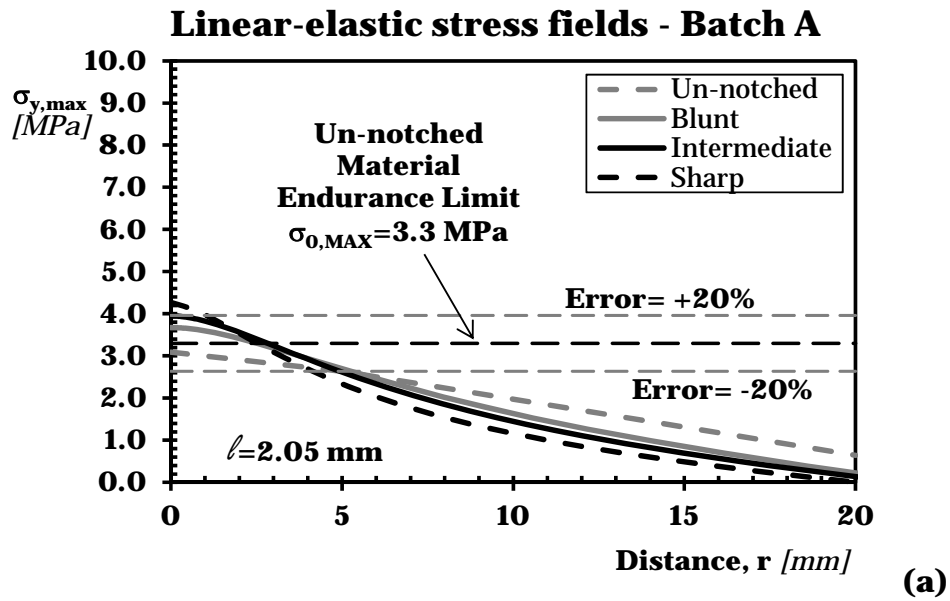
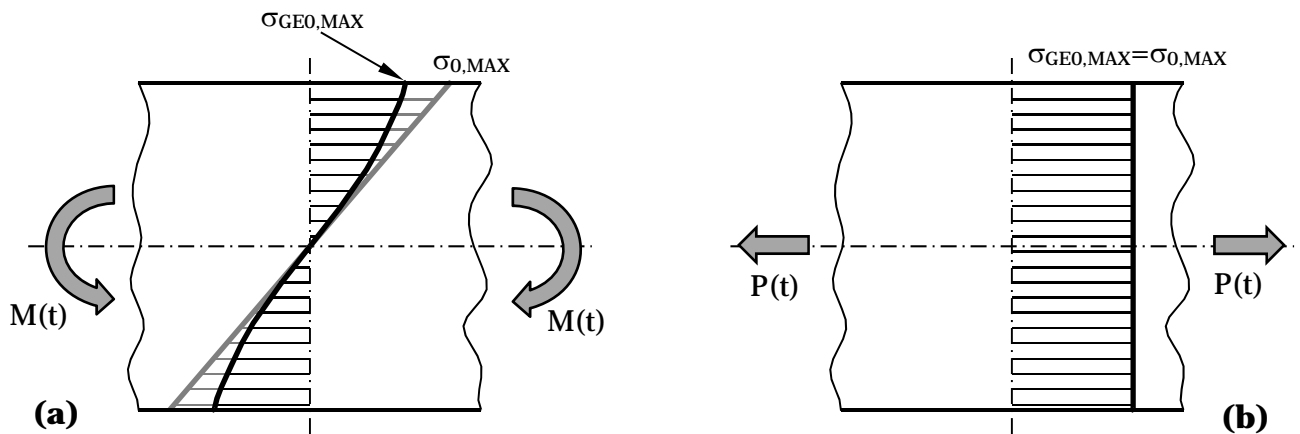
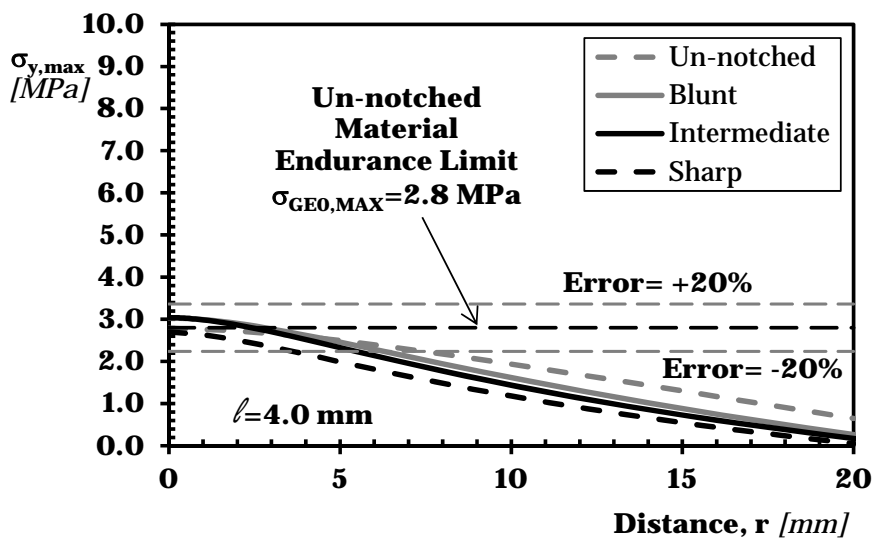


**Figure 8.** Gradient-enriched stress fields in the endurance limit condition and accuracy of GE applied according to the TCD in estimating the high-cycle fatigue strength of the tested notched concrete.

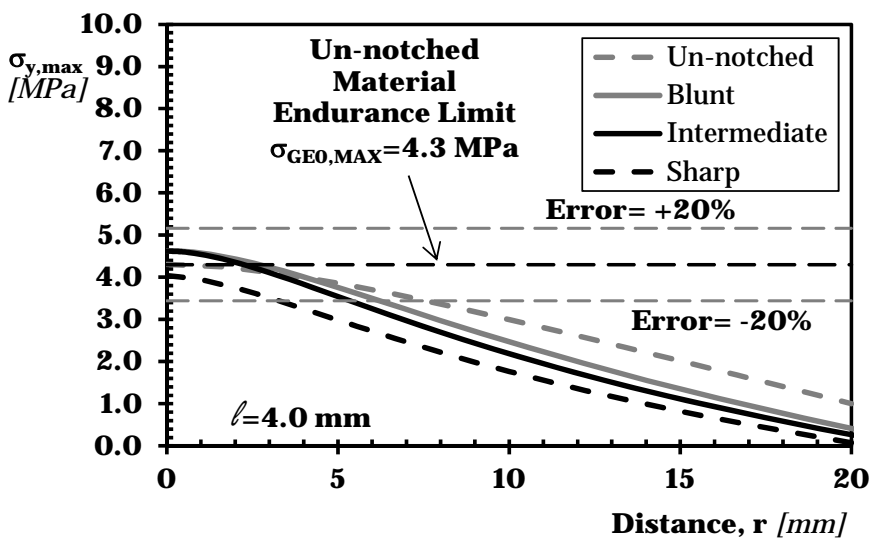


### Linear-elastic stress fields - Batch A



(c)

### Linear-elastic stress fields - Batch B



(d)

**Figure 9.** Continuum mechanics vs. gradient-enriched stress fields in a beam subjected to cyclic bending (a) as well as to cyclic axial loading (b); accuracy of GE calibrated via the average inter-aggregate distance in estimating the high-cycle fatigue strength of the tested notched concrete (c, d).